JOURNAL OF CATALYSIS 108, 467–479 (1987)

Ammonia Synthesis over a Supported Iron Catalyst Prepared from an Amorphous Iron-Zirconium Precursor

III. Mechanism of Nitrogen Adsorption and Ammonia Synthesis Kinetics

A. BAIKER,* H. BARIS,* AND R. SCHLÖGL†

*Department of Industrial and Engineering Chemistry, Swiss Federal Institute of Technology (ETH), ETH-Zentrum, CH-8092 Zürich, Switzerland; and †Fritz Haber Institut der Max Planck Gesellschaft, 1000 Berlin 33, Federal Republic of Germany

Received February 10, 1987; revised April 21, 1987

Photoemission studies (UPS and XPS) of nitrogen adsorption on amorphous $Fe_{91}Zr_9$ at 79 K indicate the presence of both molecular and atomic nitrogen on the surface. Atomic nitrogen is found to be the reactive intermediate in ammonia synthesis catalyzed by this material. Upon addition of small amounts of hydrogen to the surface covered with atomic nitrogen, this species is desorbed, presumably as NH_3, leaving nondissociated dinitrogen behind. The results of the UPS and XPS studies, including binding energies and line profiles, agree well with the results of similar investigations carried out on single crystal surfaces of iron. This supports the view that the active component of the amorphous iron-zirconium alloy is elemental iron and that the local electronic structure of the adsorption sites in elemental iron and in the amorphous alloy surface are similar. The question as to whether an amorphous surface exhibits different adsorption characteristics than a crystalline surface is discussed in the light of the nitrogen adsorption results. The findings of the photoemission studies are supported by a kinetic study of ammonia synthesis over the catalyst prepared from the amorphous alloy. Kinetic experiments were carried out in a continuous fixed-bed tubular reactor in the range 623–723 K and at 4 bar total pressure. The experimental results could be well described with a kinetic model based on the assumption that *N is the most abundant reaction intermediate. The activation energy of nitrogen adsorption derived from the kinetic data amounts to 85 kJ/mol. This value agrees well with activation energies reported in the literature for ammonia synthesis over unpromoted iron and supports the conclusion that elemental iron is the active component of the catalyst prepared by *in situ* activation of amorphous $Fe_{91}Zr_9$.

INTRODUCTION

Recently we have shown that amorphous iron-zirconium alloys constitute interesting precursors for the preparation of active ammonia synthesis catalysts (*1*). Catalysts which exhibit a high ammonia synthesis activity have been prepared by *in situ* activation of the amorphous precursor under ammonia synthesis conditions. During this activation, the amorphous precursor is irreversibly transformed by a sequence of processes, such as crystallization, segregation, and chemical reactions in the bulk and at the surface. The genesis of the active catalyst has been studied by means of several techniques, including X-ray diffraction (XRD), differential scanning calorimetry (DSC), Mössbauer spectroscopy, photoelectron spectroscopy (XPS and UPS), scanning electron microscopy (SEM), and scanning tunneling microscopy (STM). The results of these investigations, which have been reported in two previous communications (*2, 3*), indicate that the active component of the catalyst is iron stabilized by poorly crystalline zirconia. The iron exists in different forms, predominantly as stacks of disk-shaped particles and as well-developed crystals. Both morphologies are uncommon in conventional ammonia synthesis catalysts.

0021-9517/87 $3.00

Ammonia synthesis on iron is the best-established case of a structure-sensitive reaction and by far the best understood. Studies by Boudart's group on supported iron catalysts showed marked differences in the turnover rate, depending on the iron particle size (*4, 5*). Mössbauer spectra of the supported particles evidenced that an influence on the kinetics caused by metal–support interaction could be excluded, and it was suggested that the different turnover rates are solely attributed to a different surface concentration of atoms with a coordination number equal to 7, as found on the (111) faces of iron. These findings on supported iron have been confirmed recently by Spencer *et al.* (*6*) in a study of ammonia synthesis at about 20 bar on single crystals of iron.

Our previous studies (*2, 3*) have indicated that the higher activity of the iron in the catalyst obtained from the amorphous iron-zirconium precursor, as compared to polycrystalline iron, has to be attributed to its structural properties only, and not to an electronic effect which may have been caused by the existence of an amorphous or crystallized iron-zirconium alloy as the active form of the catalyst. This makes the study of nitrogen adsorption and ammonia synthesis kinetics over this catalyst an attractive objective. With this in mind we have attempted in this work to gain some information about the mechanism and the kinetics of ammonia synthesis over the amorphous precursor and the catalyst prepared from it.

EXPERIMENTAL

Amorphous $Fe_{91}Zr_9$ was prepared as ca. 0.5-cm-wide ribbons of ca. 30 μm thickness using the conventional melt spinning technique. Batches of ca. 20 g were obtained from premelted alloys in a high-vacuum environment. Ribbons of polycrystalline iron which were used as a reference in the kinetic tests were prepared by the same technique. For the kinetic experiments, the ribbons were cut into small pieces of about 1–2 cm length. Generally, 10 g of the material was stuffed into the reactor tube of 1.5 cm inner diameter, resulting in a catalyst bed length of about 15 cm. The *in situ* activation of the amorphous precursor as well as the chemical and structural changes occurring during activation have been described in our previous reports (*2, 3*). Kinetic tests were started after the *in situ* activation was completed, e.g., after the catalyst exhibited stationary activity for several hours.

The apparatus used for the kinetic measurements consisted essentially of a tubular reactor, a gas delivery system, and an infrared analyzer for ammonia (Maihak, Unor 6). The 40-cm-long stainless steel fixed-bed tubular reactor was installed in a heated air bath. Before entering the reactor, the synthesis gas was mixed and preheated in a separate preheater section. The temperature in the catalyst bed was measured by a chromel–alumel thermocouple well inserted in the center of the catalyst bed and could be held within ± 2 K. Blank tests carried out without catalyst confirmed that the empty reactor did not exhibit significant ammonia synthesis activity under the conditions used. Reactant gas flows to the reactor were controlled by thermal mass flow controllers (Brooks 5841). Hydrogen (99.999) was further purified by passing it through a Deoxo hydrogen purifier and, finally, through a drying column packed with Drierite. Nitrogen (99.995) was purified from oxygen traces by passing it through an Ascarite column, a hot copper filled furnace, and, finally, through a column packed with Anhydrone. Preliminary tests with different flow rates of the reactant feed indicated that a flow rate of about 40 ml (STP)/min was high enough to avoid any influences on the kinetics caused by nonideal flow patterns (back-mixing). The kinetic results presented in this report were obtained at a constant feed rate of 40 ml (STP)/min and at 400 kPa total pressure. The data were collected in the temperature range 623–723 K at different ratios of

N_2/H_2. Stationary activity of the catalyst during the kinetic tests was confirmed by repetition of the first measurements, after completion of the whole test series.

Photoemission studies of nitrogen adsorption were carried out in a Leybold LHS 10 electron spectrometer operating at 10^{-10} Torr base pressure. XPS and UPS data could be recorded from samples under various gaseous environments and temperatures between 80 and 900 K. Clean surfaces were obtained by Ar ion sputtering at 80 K. UPS data are presented without data treatment, and the XPS results were processed by background substraction and digital smoothing on a DS 5 computer system before presentation.

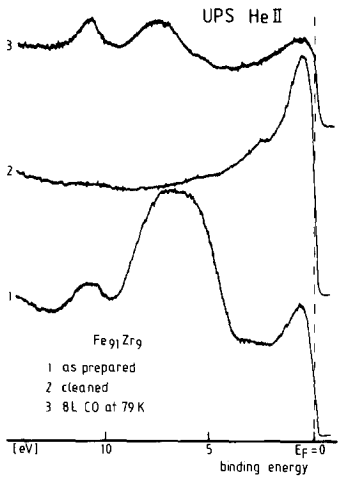

FIG. 1. UPS helium II spectra from amorphous precursor surfaces all at 79 K. Note the loss of the feature at the Fermi edge upon CO adsorption.

RESULTS

1. Photoemission Studies of Nitrogen Adsorption on an Amorphous Precursor

It is well known that dissociative adsorption of molecular nitrogen is the rate-determining step in ammonia synthesis over iron. In this section, we compare the nitrogen adsorption behavior of the alloy-derived catalysts with the known phenomena over more conventional systems such as iron single crystals. Since we are dealing with at least binary systems, complicating effects, such as several adsorption sites and less well-defined top surfaces, have to be taken into account. It was only possible to study the low-temperature sputter-cleaned surface of the amorphous precursor, since the presence of a sizable amount of oxygen on all other surfaces prevented the detection of any sign of nitrogen adsorption at 79 K and at exposures of up to 20.000 Langmuir. This inhibiting effect of preadsorbed oxygen has been described in similar systems also (*7–9*).

In Fig. 1 we compare the He II UPS data for an as-cast surface of $Fe_{91}Zr_9$ with its sputter-cleaned surface and with the surface after adsorption of approximately one monolayer of CO. This CO adsorption experiment was carried out for obtaining reference data to the successive N_2 adsorption experiments. Both molecules give rise to essentially similar spectra since they are isoelectronic. Taking into account the vastly different sticking coefficients for the two molecules, small impurities of CO may easily perturb the results of nitrogen adsorption.

The intensity of the Fe 3*d* band (at the Fermi edge) is significantly reduced upon CO chemisorption but remains almost unaffected by N_2 adsorption. This difference serves thus as criterion for distinction of CO and N_2 covering the surface. The reason for the drop in intensity of the Fe 3*d* band upon CO adsorption is presumably the formation of a covalent interaction between iron and CO which reduces either the cross section of the Fe 3*d* electrons for the UPS experiments or directly the density of states near the Fermi level. This latter explanation which is not a spectroscopic but a real chemical effect is strongly supported by the observation of a change in the shape of the Fe 3*d* peak at exposures to CO of below one Langmuir.

The central spectrum in Fig. 1 is typical of a clean iron surface. The feature containing the Fermi edge is the iron 3*d* band with a weak structure at ca. 2.7 eV, indicative of

the cleanliness of the surface (*7, 10*). Alloying with Zr causes no significant *d* band shift, and the partial density of states for Zr is barely visible due to its essentially featureless energy distribution (*11*). The surface is free of oxygen as indicated by the absence of a structure at 5.5 eV. This is important since oxygen influences the interaction of both nitrogen and ammonia with the iron surface (*8, 12*).

The oxide structure is the dominant feature in the lower trace of Fig. 1. The air-exposed surface is covered with an oxide layer. The oxide reduces the density of states at the Fermi edge significantly. The additional peak at ca. 11 eV arises from adsorbed CO. It represents the 4 σ emission. The second CO peak from the 5 σ/1 π emission is covered under the oxide structure. The undisturbed spectrum of CO on this surface can be seen in the top trace of Fig. 1. The exact binding energies of 7.6 eV for 5 σ/1 π, and 10.9 eV for 4 σ match well with literature values (*13*). The chemisorption of CO involves very strongly the iron 3*d* orbitals, and thus dramatically reduces the density of states near the Fermi edge (compare traces 2 and 3 in Fig. 1). The comparison of the intensities from the adsorbate and the height of the Fermi edge yields information on the strength of the adsorbate–substrate interaction, and allows one to distinguish between CO and N_2. Adsorption of monoatomic nitrogen species such as atoms, NH, or NH_2 involves a strong bonding interaction with the nitrogen lone pair and the iron 3*d* orbitals, and, therefore, also reduces the density of states at the Fermi edge (*7, 9*).

In Fig. 2, a sequence of events is shown which occurs during adsorption and heating of the clean surface with nitrogen. Both adsorption and heating were done in an ambient atmosphere of nitrogen which was required due to the low sticking probability of nitrogen.

In the bottom trace the spectrum of adsorbed molecular nitrogen can be seen. It differs from the spectrum of adsorbed CO

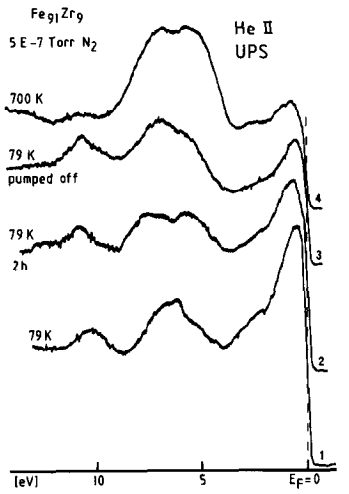

FIG. 2. Adsorption of nitrogen onto a clean alloy surface. Note the shifts of the 4 σ line (left) and the 5 σ/1 π structure (center) with time. Heating (top trace) results in oxidation of the surface (see text).

mainly by the still present structure of the iron 3*d* orbitals: molecular nitrogen interacts only weakly with the surface. The binding energies for the 4 σ orbital is 10.3 eV, and for the 5 σ/1 π orbital it is 6.8 eV. We note that these values are slightly smaller than those of the corresponding CO peaks.

Prolonged exposure of the surface to nitrogen and to hydrogen present in the residual gas of the UHV system causes the spectrum to change to the type as displayed in the second trace of Fig. 2. The 4 σ peak shifts to higher binding energy (10.9 eV) and the 5 σ/1 π peak splits into two components at 5.4 and 8.0 eV. The intensity of the Fermi edge is also reduced. We ascribe these changes to the successive contamination of the surface with a submonolayer coverage of CO and the formation of a dissociated species of nitrogen. Comparison with the literature (*9*) would allow the assignment of the split peak to the presence of NH (peaks at 5.2 and 8.4 eV) besides N_2. Atomic nitrogen would give rise to a single peak at ca. 5.0 eV (*7, 9*). The difference in the binding energy is not significant enough to decide between the presence of either N_2 and NH, or N_2, N, and traces of CO (peak

at 8 eV 5 σ CO). The latter assignment is more in line with the XPS data presented below. These allow an unambiguous distinction between atomic nitrogen and NH. Note that no indication of NH was found in these experiments.

The diffuse structure around 11 eV and the poor separation of the two main peaks point to the additional presence of molecular nitrogen on the surface. The possible alternative assignment of the whole spectrum to an admixture of CO and oxygen was excluded by surface titration experiments with CO and oxygen: at comparable coverages with these adsorbates the Fermi edge structure was completely absent.

These titration control experiments also allow one to exclude the mixture of CO and oxygen as an explanation for the spectrum obtained after termination of the exposure to nitrogen and pumping down to the base pressure of the system. The increased intensities of the structures around 11.2 and 7.4 eV may be ascribed to molecular ammonia which is prevented from being desorbed by the interruption of the supply with educts. After pumping for several hours the intensity of the two structures was reduced by ca. 50%, which is further indication that not only CO is present. We state that our binding energies are similar to previous observations (*7*) (7.4 and 11.8 eV) and that the reduced energy difference (4.2 eV, 4.4 eV in (*7*)) of the two orbitals relative to gaseous ammonia (6.0 eV) points to an increased interaction of the nitrogen lone pair with the substrate. The binding energy value for NH_3 takes into account the work function of the solid substrate which reduces the binding energy for free molecular ammonia by an estimated value of 4.7 eV.

Attempts to study the dissociation of nitrogen at the practical reaction temperature of 700 K were only partly successful. The spectrum in the top of Fig. 2 is a typical result. It resembles the spectrum of the as cast surface (Fig. 1, trace 1). The heat treatment caused oxygen to diffuse from the bulk of the sample to the surface. This gives rise to most of the intensity around 5.5 eV, and to the loss of iron *d* band intensity. XPS showed, however, both the presence of oxygen and small amounts of atomic nitrogen. Its UPS fingerprint (at ca. 5.0 eV) is hidden under the oxygen 2*p* orbital peak at ca. 5.5 eV. We state that at reaction temperature and in the presence of a large amount of oxygen we still were able to detect the same precursor species of atomic nitrogen as in the low-temperature experiments. This process is eliminated in studies with conventional substrates by several heating/sputtering cycles during sample preparation. With amorphous alloys such cleaning procedures are inadequate since they lead to irreversible changes (crystallization and segregation) of the material.

Comparison of the spectra of the as cast surface with that of the surface heated in nitrogen by the difference technique revealed four peaks of residual intensity, two of them being due to a difference in coverage with CO (less on the heated surface), and two occurring at ca. 5.0 and 2.4 eV. These peaks were also found in similar experiments with iron single crystals (*7*) and assigned to the presence of atomic nitrogen.

In order to support the interpretation of the UPS data a similar series of experiments was carried out using XPS N 1*s* spectra as an analytical tool. These spectra have the advantage of showing only nitrogen species unambiguously, but suffer from very low intensity (accumulation over 6 h per spectrum) and poor resolution. The results are summarized in Fig. 3.

Both spectra were obtained during exposure of clean alloy surfaces to a static pressure of 5×10^{-7} Torr nitrogen at 79 K. To obtain a maximum of photoelectrons the analyzer was operated in the constant retarding ratio mode. We note that under these conditions the resolving power was insufficient to see peak splittings as demonstrated in Ref. (*8*). The spectral intensity is relatively poor because the surface con-

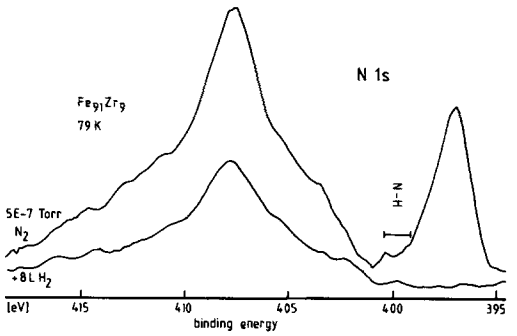

FIG. 3. XPS of adsorbed nitrogen; top trace: sample under static nitrogen pressure; bottom trace: after admission of hydrogen to the static nitrogen atmosphere. The instrumental resolution had to be limited to 1.5 eV in order to collect each spectrum within 6 h.

tained elements other than Zr (see Ref. (*2*)) and was in an undefined state with respect to the orientation of the iron faces exposed to dinitrogen. Furthermore, the metastable nature of the substrate did not allow us to apply a conventional cleaning procedure involving heat treatment.

The top trace shows two structures, the wide one is ascribed to molecular adsorption of dinitrogen in the (γ) state. The final state structure of this peak (8) is not resolved, giving rise to the large linewidth. The possible presence of (α) nitrogen (peak around 400 eV) may further broaden the line. The second narrow structure clearly indicates the presence of atomic (β) nitrogen which is believed to represent a surface nitride (*15*). The width of this line is determined by the analyzer broadening. The difference in lineshape of the two peaks is caused by the additional presence of many body effects in the spectrum of adsorbed molecular nitrogen (*8*).

In order to study the reactivity of this surface species, 8 Langmuir of hydrogen was admitted still at low temperature with the nitrogen supply terminated. The resulting spectrum is shown in the bottom trace of Fig. 3. The predominant nitrogen species on the surface is now molecular dinitrogen with all atomic nitrogen being lost. There is no evidence for hydrogenated nitrogen intermediates on the surface (peaks between the position of (β) N* and ca. 401 eV could be indicative). We suggest that the atomic N* has initially reacted to ammonia. During 4 h of data accumulation we lost the adsorbed ammonia. This experiment was reproduced several times. We are aware of the fact that the conditions of our experiments do not allow one to interpret this result unambiguously, since both experimental (desorption under X-ray irradiation and/or reaction with contaminants) and surface chemical reasons (adsorption of hydrogen at the ammonia sites and no subsequent formation of N* from adsorbed dinitrogen due to the lack of an N_2 partial pressure) may serve as explanations. However, we do conclude that (β) atomic nitrogen was the reactive precursor for the formation of the product, which was presumably ammonia.

2. *Ammonia Synthesis Kinetics*

Ammonia synthesis kinetics could only be studied over the active catalyst, since the amorphous $Fe_{91}Zr_9$ precursor was not stable under ammonia synthesis conditions and transformed slowly into the active catalyst (*2, 3*). The experimental kinetic results are listed in Table 1 and compared with kinetic data obtained over polycrystalline iron ribbons which were similarly pretreated and prepared using the same melt spinning technique. Note the significantly higher ammonia synthesis activity of the $Fe_{91}Zr_9$ catalyst as compared to the similarly pretreated polycrystalline iron ribbons. The higher activity of the $Fe_{91}Zr_9$ catalyst cannot be attributed to a different level of contamination of the two catalysts, since experiments were performed similarly over both materials. Preliminary tests with respect to possible influences on the kinetics caused by internal and external mass and heat transfer limitations (*16*) confirmed that such limitations could be ruled out under the conditions used in the kinetic measurements.

TABLE 1

Experimental Kinetic Data for Ammonia Synthesis over Catalysts Prepared from Amorphous $Fe_{91}Zr_9$

T (K)	$N_2:H_2$ (−)	$Fe_{91}Zr_9$		Fe	
		$\eta \times 10^3$ (−)	r (nmol/m^2 sec)	$\eta \times 10^3$ (−)	r (nmol/m^2 sec)
623	1:1	1.76[a]	6.28		
623	1:3	1.18	5.45		
623	3:1	3.09	4.77	No activity	
623	1:2	1.31	5.86		
623	2:1	2.44	5.46		
653	1:1	6.04	13.64	0.72	0.51
653	1:3	4.55	13.37	0.28	0.27
653	3:1	12.13	11.88	1.12	0.35
653	1:2	4.80	13.62	0.14	0.13
653	2:1	9.22	13.09	0.96	0.43
693	1:1	23.42	30.56	6.48	2.69
693	1:3	14.41	24.42	3.62	1.94
693	3:1	35.73	20.20	15.69	2.82
693	1:2	17.71	29.05	3.66	1.91
693	2:1	31.93	26.19	10.81	2.81
723	1:1	41.39	37.11	14.61	4.15
723	1:3	27.88	32.47	6.56	2.43
723	3:1	64.30	24.96	30.22	3.72
723	1:2	32.68	36.82	8.35	2.99
723	2:1	54.90	30.69	20.58	3.65

Note. Kinetic results of similarly pretreated polycrystalline iron are listed for comparison.

[a] $\eta = (NH_3)/(NH_3)_{eq.}$, where (NH_3) is the ammonia partial pressure measured at the reactor outlet, and $(NH_3)_{eq.}$ corresponds to the equilibrium pressure of ammonia at the conditions used.

Principal questions we addressed in our kinetic study were: What is a suitable kinetic model for the description of ammonia synthesis over the $Fe_{91}Zr_9$ catalyst? How do the parameters extracted from the kinetic data compare with corresponding data obtained over unpromoted iron catalysts reported in the literature? To answer these questions we have analyzed the experimental kinetic data (Table 1) using the rate expressions set up by Ozaki *et al.* (*17*), extended by taking into account the backward reaction. These rate expressions are based on the assumption that dissociative nitrogen adsorption or associative desorption is the rate-determining step (symbol $\wedge$) on a uniform surface, the most abundant reaction intermediate (*mari*) of which is either *N or *NH in equilibrium with H_2 and NH_3 (symbol 0 for zero net rate):

$$N_2 + 2* \underset{\vec{k}}{\overset{\vec{k}}{\rightleftharpoons}} 2\,*N$$

$$NH_3 + * \overset{K}{\rightleftharpoons} *N + \tfrac{3}{2}\,H_2$$

$$\text{or} \quad NH_3 + * \overset{K'}{\rightleftharpoons} *NH + H_2$$

Figure 4 shows qualitatively the potential energy profile of the overall reaction $3H_2 + N_2 = 2NH_3$ with the overall equilibrium constant K_0. The two rate equations are obtained from the following one where

quantities between curved brackets denote partial pressures:

$$r = \frac{\vec{k}(N_2)[1 - K_0^{-1}(NH_3)^2/(H_2)^3(N_2)]}{[1 + K\ddagger(NH_3)/(H_2)^n]^2}. \quad (1)$$

In Eq. (1), r is the reaction rate based on unit surface area and expressed in nmol/m^2 sec, and $K\ddagger$ stands for either K or K', depending on whether n is 1.5 for *N as *mari*, or 1 for *NH as *mari*, respectively.

In view of the low value of the ammonia equilibrium partial pressure, (N_2) and (H_2) may be put approximately equal to $(N_2)_{eq.}$ and $(H_2)_{eq.}$, respectively. With these simplifications, the efficiency $\eta = (NH_3)/(NH_3)_{eq.}$ and the parameter $\gamma = (H_2)/0.75p$, the integration of Eq. (1) through the catalyst bed leads to Eq. (2) in which the dimensionless numbers α and β are defined differently, depending on whether *N or *NH is *mari*, respectively:

$$0 = 1 - \alpha\left[\frac{1}{2}(1 + \beta^2) \ln\left(\frac{1 + \eta}{1 - \eta}\right) - \beta \ln(1 - \eta^2) - \eta\right]. \quad (2)$$

For *N as *mari*, α and β are given by Eqs. (3) and (4), respectively,

$$\alpha = (\tfrac{1}{4})(\tfrac{3}{4})^{1.5} \frac{VT}{RT_R^2 S_{BET} w_K} p^2 \frac{K_0^{1.5}K^2}{\vec{k}} \gamma^{1.5}(4 - 3\gamma)^{0.5} \quad (3)$$

$$\beta = \frac{2}{K[K_0(4 - 3\gamma)p]^{0.5}}. \quad (4)$$

In the case where *NH is *mari*, α and β are defined by Eqs. (5) and (6), respectively,

$$\alpha = (\tfrac{1}{4})(\tfrac{3}{4})^{2.5} \frac{VT}{RT_R^2 S_{BET} w_K} p^3 \frac{K_0^{1.5}K'^2}{\vec{k}} \gamma^{2.5}(4 - 3\gamma)^{0.5} \quad (5)$$

$$\beta = \frac{2}{K'p[(\tfrac{3}{4})K_0(4 - 3\gamma)\gamma]^{0.5}}, \quad (6)$$

where T is the temperature in the catalyst bed (K); T_R is the standard temperature (273 K); V is the total feed flow rate (cm^3(STP)/sec); R is the gas constant (cm^3 kPa/mol K); p is the total pressure (kPa); w_k is the total weight of the catalyst (g); S_{BET} is the BET surface area of the catalyst (m^2/g).

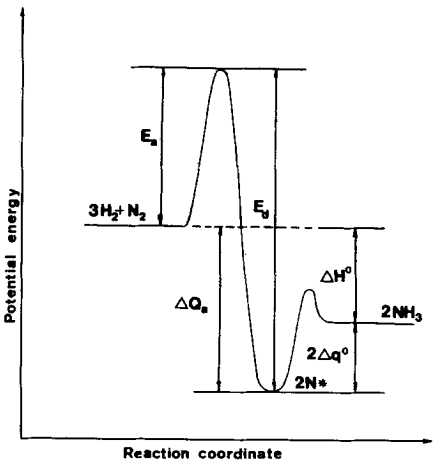

FIG. 4. Qualitative potential energy profile of the reaction.

The calculations of the overall equilibrium constants K_0 were based on those carried out by Schulz and Schaefer (*18*).

A nonlinear multiresponse regression program (*19*) was used to search for the parameters $\vec{k}$ and K (or K') which statistically yield the best accordance (maximum likelihood (*20*)) between the experimental and the calculated responses η. The parameters estimated for the two models are summarized in Table 2 along with the corresponding "t_Φ" values,

$$t_\Phi = \Phi/S(\Phi), \quad (7)$$

and the residual sum of squares (RSS),

$$RSS = \sum_{i=1}^{n} (\eta_{i,calc} - \eta_{i,exptl})^2, \quad (8)$$

where Φ is the estimated parameter value and $S(\Phi)$ its standard deviation.

Comparison of the residual sum of squares obtained for the two rate equations (Eqs. (1) and (2)) based on different *mari* indicates that the assumption of *N leads to a significantly better fit of the kinetic data. Furthermore, the application of rate ex-

TABLE 2

Estimated Kinetic Parameters Using the Models Based on *N and *NH, Respectively

Temp. (K)	Surface $N_2:H_2$ (−)	$\eta \times 10^3$ (−)	*mari* *N estimated parameters $\vec{k}$ [$kPa^{-1}\ sec^{-1}$] K [$kPa^{0.5}$]	*mari* *NH estimated parameters $\vec{k}$ [$kPa^{-1}\ sec^{-1}$] K'[−]
623	1:1	1.76	$\vec{k} = 0.257 \times 10^{-4}$	$\vec{k} = 0.270 \times 10^{-4}$
	1:3	1.18	(24.86)[a]	(12.22)
	3:1	3.09	$K = 18.96 \times 10^4$	$K' = 2.671 \times 10^4$
	1:2	1.31	(24.92)	(18.04)
	2:1	2.44	$RSS_b = 2.21 \times 10^{-8}$	$RSS = 5.33 \times 10^{-8}$
653	1:1	6.04	$\vec{k} = 0.470 \times 10^{-4}$	$\vec{k} = 0.455 \times 10^{-4}$
	1:3	4.55	(5.80)	(5.63)
	3:1	12.13	$K = 5.732 \times 10^4$	$K' = 0.849 \times 10^4$
	1:2	4.80	(4.78)	(6.98)
	2:1	9.22	$RSS = 4.52 \times 10^{-6}$	$RSS = 3.59 \times 10^{-6}$
693	1:1	23.42	$\vec{k} = 1.397 \times 10^{-4}$	$\vec{k} = 1.363 \times 10^{-4}$
	1:3	14.41	(32.05)	(6.16)
	3:1	35.73	$K = 4.012 \times 10^4$	$K' = 0.533 \times 10^4$
	1:2	17.71	(32.26)	(8.90)
	2:1	31.93	$RSS = 2.26 \times 10^{-6}$	$RSS = 3.21 \times 10^{-5}$
723	1:1	41.39	$\vec{k} = 2.311 \times 10^{-4}$	$\vec{k} = 2.310 \times 10^{-4}$
	1:3	27.88	(44.80)	(2.86)
	3:1	64.30	$K = 4.407 \times 10^4$	$K' = 0.549 \times 10^4$
	1:2	32.68	(51.40)	(4.53)
	2:1	54.90	$RSS = 4.37 \times 10^{-6}$	$RSS = 3.26 \times 10^{-4}$

[a] Values given in parentheses are t_Φ values (Eq. (7)) of estimated parameters.
[b] Residual sum of squares as defined in Eq. (8).

pression (2) based on the assumption of *NH being *mari* does not yield significant parameters $\vec{k}$ and K', as is indicated by the low t_Φ values obtained for these parameters. The low t_Φ values are due to the high correlation between $\vec{k}$ and K'. Thus, the present kinetic data could only meaningfully be described by rate expression (1) based on *N as *mari*.

Figure 5 depicts the Arrhenius plot of the adsorption rate constant $\vec{k}$ and the Van't Hoff plot of the equilibrium constant K, as obtained by analyzing the kinetic data with rate expression (1) based on *N being *mari*. From these plots we calculate by linear regression the activation energy of nitrogen adsorption $E = 85 \pm 5$ kJ/mol, and the heat of ammonia adsorption ($NH_3 + * = *N + \frac{3}{2} H_2$), $\Delta q_0 = 53 \pm 20$ kJ/mol. In turn, an estimate of the heat of adsorption of nitrogen, ΔQ_a, corresponding to $N_2 + 2* \rightarrow 2\ *N$ can be obtained readily from Δq_0 using $\Delta Q_a = 2\Delta q_0 - \Delta H_0$, where ΔH_0 is the overall reaction enthalpy at mean reaction temperature (673 K). Using this relationship we estimate $\Delta Q_a = 206$ kJ/mol. Note that both Δq_0 as well as ΔQ_a could be estimated from our kinetic data only with little confidence, due to the limited number of experiments and the relatively large standard deviation of Δq_0.

DISCUSSION

The UPS model experiments showed the occurrence of the adsorption and dissociation processes of molecular nitrogen at

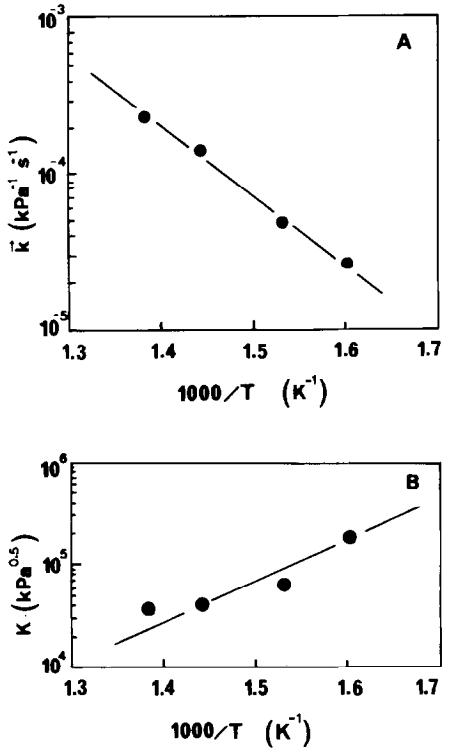

FIG. 5. Results of ammonia synthesis kinetics measured over catalysts prepared by *in situ* activation of the amorphous precursor. (A) Arrhenius plot of nitrogen adsorption rate constant $\vec{k}$ (correlation coefficient (*21*) of linear regression, $R = 0.996$); (B) Van't Hoff plot of the equilibrium constant for the adsorption of ammonia $NH_3 + * \rightleftharpoons N^* + \frac{3}{2} H_2$ (correlation coefficient $R = 0.87$).

low temperatures. The desorption of atomic nitrogen after exposure to hydrogen which did not cause desorption of coadsorbed molecular nitrogen indicates that the atomic nitrogen is the immediate precursor for ammonia formation. These results and even the adsorption kinetics of N_2 are fully in agreement with the reaction mechanism accepted for iron single crystal surfaces (*7, 9*). There is also good agreement in the binding energies of the various molecular orbitals involved. We conclude that it is essentially elemental iron which is the active component in the ammonia synthesis, at least under the reaction conditions of our UHV experiments. This conclusion and the observation of atomic nitrogen at reaction temperature also justify the extention of the UHV results to our catalytic tests at higher pressures and temperatures, where all analytical results (*2, 3*) indicate that only iron is present as a metal.

The negligible influence of the presence of zirconium is in agreement with the very small *d* band shift of the iron: the electronic structure of this iron zirconium alloy is very similar to that of elemental iron. In the nickel zirconium alloys mentioned above this is not the case: here a significant alteration of the electronic structure of the alloy relative to the element is strongly reflected in the chemisorption properties (*13*). The experimental evidence is less rigorous in the present case than in the studies with single crystals. This arises from the experimental constraints imposed by the limited stability of our substrates. But only the study of the genuine alloy surface allowed us to reach the conclusions drawn above. We want to point out that the results presented above were well reproducible with several samples of different alloys. In some cases the iron to zirconium ratio was changed, but overall very few changes occurred, taking into account the difference in the iron atomic surface concentration. In particular, no evidence for the formation of significant amounts of zirconium nitrides was found with alloys as rich as $Fe_{36}Zr_{64}$.

Our XPS results show the presence of both molecular and atomic nitrogen on the surface. Atomic nitrogen is a reactive intermediate for the synthesis of ammonia. The failure to detect any hydrogenated species as seen in the UPS results may be explained by the long accumulation time which allows, for instance, the replacement of these minority species by more strongly bound species. The binding energies and line profiles again agree quite well with the results from single crystals of iron (*8*), indicating once more the similarity of the local electronic structure of the adsorption sites in elemental iron and the alloy surface. This conclusion gives us further justification to

apply the results of the UHV model experiments to the catalytic experiments under realistic conditions.

An interesting point which should be considered, when discussing the nitrogen adsorption results obtained, is the question as to whether an amorphous surface can exhibit different adsorption characteristics than a polycrystalline surface. This question arises in the present contribution, since our working catalyst is largely polycrystalline, whereas the adsorption studies were performed on amorphous alloy surfaces.

It is well established that ammonia synthesis and nitrogen adsorption are structure-sensitive reactions. In our study both surfaces, i.e., the surface of the amorphous precursor as well as that of the polycrystalline catalysts, exhibited an unknown distribution of various iron crystal faces. Significant differences in this distribution or a different surface composition (we are discussing a binary alloy liable to segregation) of the two types of surfaces may result in different adsorption properties. The topography of the surfaces (see Ref. (*3*)) differed in many respects, in particular, the working catalyst showed a marked anisotropy in the crystal face distribution. Thus differences in the amount of adsorbed nitrogen per unit surface area are likely to occur. In electron spectroscopy this may result in a too low nitrogen coverage of the amorphous surface (broad distribution of active and inactive sites) to serve as a suitable quantitative model for the nitrogen coverage of the working catalyst.

More important for the discussion of the spectroscopic results is, however, a possible qualitative difference of the two surfaces in their chemisorption behavior. Evidence for this emerges from a recent comparative study (*13*) of CO adsorption on amorphous Ni–Zr alloys and on the surfaces of the polycrystalline alloy constituents. In this work the observed difference in the ratio of molecular to dissociative chemisorption was related to shifts in the *d* band electronic structure of nickel in the metal relative to that in the alloy. As stated above, in our case, we did not find any difference in the iron *d* band of $Fe_{91}Zr_9$ as compared to that of α iron. Hence, we exclude any significant difference in the qualitative chemisorption behavior of nitrogen. We also did not observe any difference in the CO adsorption normalized to the number of iron sites in the surface (amount adsorbed, kinetics, chemical shift) when comparing CO adsorption on polycrystalline α iron and $Fe_{91}Zr_9$.

It may have been expected that an amorphous surface without long-range order and a cluster-like microstructure should behave differently in a structure-sensitive reaction than a crystalline surface. We interpret the similarity of the nitrogen adsorption on both surfaces as an indication for a similarity of the microstructure of the surfaces. We emphasize that both types of surfaces, i.e., the polycrystalline and the amorphous surface were extensively sputter-cleaned without any subsequent annealing. This pretreatment (cleaning) may have produced the similarity of the two surfaces (*23*). At any rate, the qualitative agreement between the nitrogen adsorption results obtained on single crystal surfaces and on our less well-defined, but more realistic, samples may help to bridge the gap between single crystal and real catalysis. The results of our kinetic studies are discussed below.

The most important result emerging from the experimental kinetic data listed in Table 1 is that the activity of the $Fe_{91}Zr_9$ catalyst exceeds that of similarly prepared and pretreated polycrystalline iron ribbons by more than an order of magnitude. Our previous investigations (*2, 3*) dealing with the physical and chemical structure of the bulk and surface of the $Fe_{91}Zr_9$ catalyst have shown us that the higher activity of iron in this catalyst is solely attributed to its unique morphology. Iron was found to exist in two prevalent forms, as stacks of disk-shaped particles and as well-developed crystals. Both these morphologies are not

found in technical ammonia synthesis catalysts.

As concerns the absolute activity of the catalyst, we can only give a rough estimate of the turnover rate, since the long exposure of the amorphous $Fe_{91}Zr_9$ alloy to the synthesis gas during activation led to considerable contamination of the surface with carbon (see Table 1 in Ref. (*2*)). Moreover, the iron concentration in the surface region as determined by XPS (*2*) does not necessarily mirror the concentration of accessible iron surface atoms. Assuming that the iron concentration of about 50% determined by XPS corresponds to the concentration of accessible iron atoms, and that the contamination with carbon did not influence the kinetic results, we estimate a turnover number of about 4 $ksec^{-1}$ for ammonia synthesis at 693 K. Note that this is a very conservative estimate, in particular, in view of the marked contamination of the surface (Table 1, Ref. (*2*)). Assignment of the absolute turnover number would require a catalyst surface which is free of contamination and the determination of the accessible iron surface atoms by chemisorption measurements.

The significantly better description (Table 2, values of RSS and t_Φ) of the kinetic data of ammonia synthesis by the model with *N as *mari* supports the conclusions emerging from the photoemission studies of nitrogen adsorption discussed above. It is also in agreement with earlier kinetic investigations of Scholten *et al.* (*24*), Kummer and Emmett (*25*), as well as Morikawa and Ozaki (*26*), who concluded from their isotope exchange experiments that on iron catalysts without an alkali promoter above 620 K, atomic nitrogen is prevalent on the surface. The activation energy of nitrogen adsorption (85 kJ/mol) calculated from our kinetic data compares well with corresponding values reported in the pertinent literature references cited above and with that found recently in kinetic studies performed over iron single crystal surfaces (*6*). Similarly, the heat of adsorption of nitrogen ($N_2 + 2^* \rightarrow 2\ ^*N$), $\Delta Q_a = 206$ kJ/mol, compares well with corresponding values reported for nitrogen adsorption on iron single crystal surfaces (*27*). However, we should keep in mind that a close comparison is impossible as these values depend very much on the coverage of the surface with nitrogen, and this in turn is controlled by the pressure applied in the kinetic experiments.

The surface nonuniformity of iron catalysts with respect to nitrogen adsorption was originally demonstrated by Scholten *et al.* (*24*). Later Boreskova *et al.* (*28*) showed by isotope exchange experiments that the apparent nonuniformity was not caused by nitrogen–nitrogen interactions on a homogeneous surface (induced nonuniformity), but by the presence of different adsorption sites on the surface. There is little question that the complete description of the kinetics of ammonia synthesis requires a treatment of the nonuniformity of the surface. However, the consistency of the present data with the rate expression based on a uniform surface (covered with *N) indicates that the nonuniform surface assumption is not a requirement for an adequate description of ammonia synthesis kinetics on this catalyst at pressures up to 4 bar. This behavior is in line with the recent findings of Stoltze and Norskov (*29*), who showed that it is possible to calculate the ammonia synthesis rate in a catalytic reactor at industrial conditions using the assumption that the surface is energetically uniform and starting from measurements of the properties of the reactants on well-defined single crystal surfaces under UHV conditions.

The treatment of our kinetic data by classical kinetics provided a good fit of the data, physically meaningful rate parameters, and, most important, it is in line with the results of the photoemission studies of nitrogen adsorption. This indicates that the mechanism of ammonia synthesis over the amorphous iron-zirconium alloy, as well as over the catalyst prepared from it, is similar to the known mechanism of this reaction over iron. All these results support the

conclusion drawn in our previous investigations (*2, 3*) that the activity of the catalyst prepared by *in situ* activation of amorphous $Fe_{91}Zr_9$ is solely attributed to metallic iron which exists in morphologies not found in conventional ammonia synthesis catalysts (*3*).

CONCLUSIONS

On amorphous $Fe_{91}Zr_9$ nitrogen is adsorbed as dinitrogen and atomic nitrogen at temperatures as low as 79 K. Upon addition of hydrogen, the atomic nitrogen desorbs, presumably as NH_3. These findings are in good agreement with corresponding results obtained on iron single crystal surfaces (*7, 9*) and indicate that the active component in the amorphous alloy is essentially elemental iron as in the catalyst prepared from it (*2, 3*).

The study of ammonia synthesis kinetics carried out over the active catalyst at a total pressure of 4 bar supports this contention. A kinetic rate expression based on the assumption that adsorbed atomic nitrogen is *mari* fits the experimental data and yields rate parameters which are similar to those reported in the literature for ammonia synthesis over unpromoted iron.

ACKNOWLEDGMENTS

Financial support by LONZA AG, Switzerland, is kindly acknowledged. One of us (R.S.) is grateful to the Swiss National Science Foundation for financially supporting his stay at the Institute of Physics at the University of Basel. Thanks are also due to Prof. G. Ertl for a critical reading of the manuscript.

REFERENCES

1. Armbruster, E., Baiker, A., Baris, H., Güntherodt, H. J., and Schlögl, R., *J. Chem. Soc. Chem. Commun.*, 299 (1986).
2. Baiker, A., Schlögl, R., Armbruster, E., and Güntherodt, H. J., *J. Catal.* **107,** 221 (1987).
3. Schlögl, R., Wiesendanger, R., and Baiker, A., *J. Catal.* **108,** 452 (1987).
4. Boudart, M., Topsoe, H., Dumesic, J. A., *in* "The Physical Basis for Heterogeneous Catalysis" (E. Drauglis, and R. I. Jaffe, Eds.), p. 337. Plenum, New York, 1975.
5. Dumesic, J. A., Topsoe, H., and Boudart, M., *J. Catal.* **37,** 513 (1975).
6. Spencer, N. D., Schoonmaker, R. C., and Somorjai, G. A., *J. Catal.* **74,** 129 (1982).
7. Grunze, M., Bozso, F., Ertl, G., and Weiss, M., *Appl. Surf. Sci.* **1,** 241 (1978).
8. Grunze, M., Golze, M., Hirschwald, W., Freund, H. J., Pulm, H., Seip, U., Tsai, M. C., Ertl, G., and Küppers, J., *Phys. Rev. Lett.* **53,** 850 (1984).
9. Weiss, M., Ertl, G., and Nitschke, F., *Appl. Surf. Sci.* **2**(4), 614 (1979).
10. Kishi, K., and Roberts, M. W., *Surf. Sci.* **62,** 256 (1977).
11. Oelhafen, P., *in* "Liquid and Amorphous Metals" (F. E. Luborski, Ed.), p. 249. Butterworths, London, 1983.
12. Shvachko, V. J., and Fogel, Y. M., *Kinet. Katal. (Engl. Ed.)* **7,** 635 (1966).
13. Hauert, R., Oelhafen, P., Schlögl, R., and Güntherodt, H. J., *Solid State Commun.* **55,** 583 (1985).
14. Ertl, G., Lee, S. B., and Weiss, M., *Surf. Sci.* **114,** 515 (1982).
15. Bozso, F., Ertl, G., Grunze, M., and Weiss, M., *J. Catal.* **49,** 18 (1977).
16. Anderson, J. R., and Pratt, K. C., "Introduction to Characterization and Testing of Catalysts," p. 268 ff. Academic Press, Orlando/London, 1985.
17. Ozaki, A., Taylor, S. H., and Boudart, M., *Proc. R. Soc. London, Ser. A* **258,** 47 (1960).
18. Schulz, G., and Schaefer, H., *Ber. Bunsenges. Phys. Chem.* **70,** 21 (1966).
19. Klaus, R., and Rippin, D. W. T., *Comput. Chem. Eng.* **3,** 105 (1979).
20. Bard, Y., "Nonlinear Parameter Estimation," p. 61. Academic Press, New York, 1974.
21. Kreiszig, E., "Statistische Methoden und Ihre Anwendungen," p. 301. Vandenhoeck & Ruprecht, Göttingen, 1975.
22. Armbruster, E., Baiker, A., Güntherodt, H. J., Schlögl, R., and Walz, B., *in* "Preparation of Catalysts IV" (P. Grange, P. A. Jacobs, and G. Poncelet, Eds.), pp. 389–400. Elsevier, Amsterdam, 1987.
23. Wiesendanger, R., Ringger, M., Schlögl, R., Brunner, A., and Güntherodt, H. J., *IBM J. Res.*, 264 (1986).
24. Scholten, J. F. F., Zwietering, P., Konvalinka, J. A., and de Boer, J. H., *Trans. Faraday Soc.* **55,** 2166 (1959).
25. Kummer, J. T., and Emmett, P. H., *J. Chem. Phys.* **19,** 68 (1964).
26. Morikawa, Y., and Ozaki, A., *J. Catal.* **12,** 145 (1968).
27. Ertl, G., Weiss, M., and Lee, S. B., *Chem. Phys. Lett.* **60,** 391 (1979).
28. Boreskova, E. G., Juchaev, V. L., Pen'kovoi, B. E., and Temkin, M. I., *Kinet. Katal.* **13,** 385 (1972).
29. Stoltze, P., and Norskov, J. K., *Phys. Rev. Lett.* **55,** 2502 (1985).